Mechanism of the Methane → Methanol Conversion Reaction Catalyzed by Methane Monooxygenase: A Density Functional Study

Harold Basch,*,† Koichi Mogi, Djamaladdin G. Musaev,* and Keiji Morokuma*

Contribution from the Cherry L. Emerson Center for Scientific Computation and Department of Chemistry, Emory University, Atlanta, Georgia 30322

Abstract: The hybrid density functional (DFT) method B3LYP was used to study the mechanism of the methane hydroxylation reaction catalyzed by a non-heme diiron enzyme, methane monooxygenase (MMO). The key reactive compound **Q** of MMO was modeled by $(NH_2)(H_2O)Fe(\mu\text{-}O)_2(\eta^2\text{-}HCOO)_2Fe(NH_2)(H_2O)$, **I**. The reaction is shown to take place via a bound-radical mechanism and an intricate change of the electronic structure of the Fe core is associated with the reaction process. Starting with **I**, which has a diamond-core structure with two Fe^{IV} atoms, $L_4Fe^{IV}(\mu\text{-}O)_2Fe^{IV}L_4$, the reaction with methane goes over the rate-determining H-abstraction transition state **III** to reach a bound-radical intermediate **IV**, $L_4Fe^{IV}(\mu\text{-}O)(\mu\text{-}OH(\cdots CH_3))Fe^{III}L_4$, which has a bridged hydroxyl ligand interacting weakly with a methyl radical and is in an $Fe^{III}-Fe^{IV}$ mixed valence state. This short-lived intermediate **IV** easily rearranges intramolecularly through a low barrier at transition state **V** for addition of the methyl radical to the hydroxyl ligand to give the methanol complex **VI**, $L_4Fe^{III}(OHCH_3)\text{-}(\mu\text{-}O)Fe^{III}L_4$, which has an $Fe^{III}-Fe^{III}$ core. The barrier of the rate-determining step, methane H-abstraction, was calculated to be 19 kcal/mol. The overall CH_4 oxidation reaction to form the methanol complex, **I** + CH_4 → **VI**, was found to be exothermic by 39 kcal/mol.

I. Introduction

The field of bioinorganic chemistry is one of the extremely active areas of chemistry, and has made tremendous progress in recent years because of improved spectroscopic techniques, the knowledge of the structure and nature of active sites and intermediates of enzyme catalyzed processes, as well as an ever-increasing crystallographic database of protein structure.[1] Among many interesting developments, the O_2-activating properties of iron-containing metalloenzymes have been widely recognized. In particular, binuclear Fe-containing metalloenzymes, such as hemerythin[2] (oxygen transport and storage), ribonucleotide diphosphate reductase[3] (RDPR, formation of a catalytically active tyrosine radical), methane monooxygenase[3a,b,4] (MMO, activation of dioxygen for insertion into the C−H bond of stable hydrocarbons), $^9\Delta$-desaturase[5] (stearoyl-acyl carrier), phenol hydroxylase,[6] xylene monooxygenase,[7] alkane hydroxylase,[7] toluene 2-monooxygenase,[8] and toluene 4-monooxygenase,[9]

have been a focus of extensive research for the past several years. Despite these efforts, the mechanisms of these catalytic reactions still remain unclear and need additional and comprehensive studies using different techniques. In the present paper we intend to study the mechanism of methane oxidation by MMO using quantum chemistry methods.

Methane monooxygenase (MMO) is an enzyme that catalyzes the methane oxidation reaction, i.e., conversion of the inert methane molecule to methanol. This is a classic monooxygenase reaction in which two reducing equivalents from NAD(P)H are utilized to split the O−O bond of O_2. One O atom is reduced to water by 2-electron reduction, while the second is incorporated into the substrate to yield methanol:

$$CH_4 + O_2 + NAD(P)H + H^+ \rightarrow$$
$$CH_3OH + NAD(P)^+ + H_2O$$
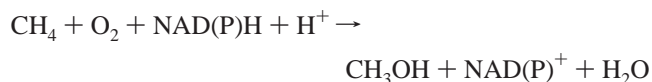
Two forms of MMO have been found, soluble and particulate. The best-characterized forms of the soluble MMO (sMMO) contain[4,10] three protein components: hydroxylase (MMOH), so-called B component (MMOB), and reductase (MMOR), each of which is required for efficient substrate hydroxylation coupled to NADH oxidation. The hydroxylase, MMOH, which binds O_2 and substrate and catalyzes oxidation, is a dimer, each half of which contains three types of subunits (α, β, γ) and a hydroxy-bridged binuclear iron cluster. In the resting state of MMOH ($MMOH_{ox}$), the diiron cluster is in the diferric state

† On sabbatical leave from Department of Chemistry, Bar Ilan University, Ramat Gan, Israel.

(1) See: *Chem. Rev.* **1996**, *96*, all papers therein.

(2) Stenkamp, R. E. *Chem. Rev.* **1994**, *94*, 715.

(3) (a) Feig, A. L.; Lippard, S. J. *Chem. Rev.* **1994**, *94*, 759. (b) Liu, K. E.; Lippard, S. J. *Adv. Inorg. Chem.* **1995**, *42*, 263. (c) Sjoberg, B.-M. S*tructure of Ribonucleotide Reductase from Escherichia coli*; Eckstein, F., Lilley, D. M. J., Eds.; Springer-Verlag: Berlin, 1995; Vol. 9, pp 192−221.

(4) (a) Waller, B. J.; Lipscomb, J. D. *Chem. Rev.* **1996**, *96*, 2625 and references therein. (b) Shu, L.; Nesheim, J. C.; Kauffmann, K.; Munck, E.; Lipscomb, J. D.; Que, L., Jr. *Science* **1997**, *275*, 515.

(5) Fox, B. G.; Shanklin, J.; Somerville, C.; Munck, E. *Proc. Natl. Acad. Sci. U.S.A.* **1993**, *90*, 2486.

(6) Nordlund, I.; Powlowski, J.; Shingler, V. *J. Bacteriol.* **1990**, *172*, 6826.

(7) Shanklin, J.; Whittle, E.; Fox, B. G. *Biochemistry* **1994**, *33*, 12787.

(8) Newman, L. M.; Wackett, L. P. *Biochemistry* **1995**, *34*, 14066.

(9) Pikus, J. D.; Studts, J. M.; Achim, C.; Kauffmann, K. E.; Munck, E.; Steffan, R. J.; McClay, K.; Fox, B. G. *Biochemistry* **1996**, *35*, 9106.

(10) (a) DeRose, V. J.; Liu, K. E.; Kurtz, D. M., Jr.; Hoffman, B. M.; Lippard, S. J. *J. Am. Chem. Soc.* **1993**, *115*, 6440. (b) Fox, B. G.; Hendrich, M. P.; Surerus, K. K.; Andersson, K. K.; Froland, W. A.; Lipscomb, J. D. *J. Am. Chem. Soc.* **1993**, *115*, 3688. (c) Thomann, H.; Bernardo, M.; McCormick, J. M.; Pulver, S.; Andersson, K. K.; Lipscomb, J. D.; Solomon, E. I. *J. Am. Chem. Soc.* **1993**, *115*, 8881.

Scheme 1. Structural Representation of the Binuclear Fe Center of Diferric MMOH$_{ox}$ and Diferrous MMOH$_{red}$ (after ref 4a)

MMOH$_{ox}$ - *M. capsulatus* (4 °C)

MMOH$_{ox}$ - *M. trichosporium* (-18 °C)
- *M. capsulatus* (-160 °C)

MMOH$_{red}$ - *M. capsulatus* (-160 °C)

[Fe^{II}−Fe^{III}], and can accept one or two electrons to generate the mixed-valence [Fe^{III}−Fe^{II}] or diferrous state [Fe^{II}−Fe^{II}], respectively. The diferrous state of hydroxylase (MMOH$_{red}$) is the only one capable of reacting with dioxygen and initiating the catalytic cycle.

X-ray crystallographic studies of the enzyme from *Methylococcus capsulatus* (Bath)[11] and *Methylosinus trichosporium* OB3b[12] have unveiled the coordination environment of the Fe centers of MMOH$_{ox}$ and MMOH$_{red}$. According to these studies (see Scheme 1), in MMOH$_{ox}$ each Fe center has a six-coordinate octahedral environment. Fe ions are bridged by a hydroxide ion, a bidentate Glu γ-carboxylate, and a water molecule (or another carboxylate). In addition, each Fe ion is coordinated by one His nitrogen ligand and one monodentate Glu carboxylate. The two Fe centers are different from each other in that one of them (Fe^2) has an additional monodentate glutamate carboxylate, while the other Fe (Fe^1) has one additional water molecule. Upon reduction, one of the carboxylate ligands undergoes a so-called "1,2-carboxylate shift" from being a terminal, monodentate ligand bound to Fe^2 to a monodentate, bridging ligand between the two irons, with the second oxygen of this carboxylate also coordinated to Fe^2. In addition, the hydroxyl bridge is lost, and the other hydroxy/water bridge shifts from serving as a bridge to being terminally bound to Fe^1. Also, the terminal water bound to Fe^1 in the oxidized form of MMOH seems to move out upon reduction of the cluster. Thus, in reduced form of MMOH$_{red}$ the ligand environment of Fe ions becomes effectively five coordinated, which is reasonable since this is the form of the cluster that activates dioxygen.

It was established[4] that MMOH$_{red}$ reacts very fast with O$_2$ and forms a metastable, so-called compound **O**, which spontaneously converts to another compound called **P** (see Scheme 2). Spectroscopic studies[13] indicate that compound **P** is a peroxide species, where both oxygens are bound symmetrically to the irons. The structure of this compound is unknown. Compound **P** spontaneously converts to compound **Q**, which was proposed to contain two antiferromagnetically coupled high-spin Fe^{IV} centers. EXAFS and spectroscopic studies[4b,14] of compound **Q**, which was trapped from *M. trichosporium* OB3b and *M. capsulatus*, have demonstrated that compound **Q** has a

Scheme 2. Experimentally Proposed Catalytic Cycle of MMO

diamond core, (Fe^{IV})$_2$(μ-O)$_2$ structure with one short (1.77 Å) and one long (2.05 Å) Fe−O bond per Fe atom and a short Fe−Fe distance of 2.46 Å. Compound **Q** has been proposed to be the key oxidizing species for MMO.

In the literature several mechanisms[4a,15] for the reaction of intermediate **Q** with alkane have been proposed, which can be divided into two different classes: (1) radical and (2) nonradical mechanisms. The radical mechanism starts with abstraction of the hydrogen atom from the substrate to form **QH** (hydroxyl bridged **Q** compound) and free alkyl radical, while the nonradical mechanism implies a concerted pathway, occurring via a four-center transition state and leading to a "hydrido-alkyl-**Q**" compound. Latest experimental studies[16] show that the mechanism of this reaction is more complex, and even could be different for the enzyme isolated from different organisms; radical clock substrate probe studies with sMMO isolated from *M. Capsulatus (Bath)* afforded no evidence for formation of substrate radical, while for enzyme isolated from *M. Trichosporium* OB3b, evidence for a substrate radical was detected. One should expect that the protein environment of the enzyme will also play a significant role in this process. Some authors even interpreted it in terms of existence of parallel reaction pathways. Thus, the elucidation of validity of different mechanisms including the structure of assumed intermediates and transition states is an open question and requires a large amount of further study. To provide some insight into these nontrivial

(11) (a) Rosenzweig, A. C.; Fredrick, C. A.; Lippard, S. J.; Nordlung, P. *Nature* **1993**, *366*, 537. (b) Rosenzweig, A. C.; Nordling, P.; Takahara, P. M.; Fredrick, C. A.; Lippard, S. *J. Chem. Biol.* **1995**, *2*, 409.

(12) Elango, N.; Radhakrishman, R.; Froland, W. A.; Waller, B. J.; Earhart, C. A.; Lipscomb, J. D.; Ohlendorf, D. H. *Protein Sci.* **1997**, *6*, 556. (b) Nesheim, J. C.; Lipscomb, J. D. *Biochemistry* **1996**, *35*, 10240 and references therein.

(13) (a) Liu, K. E.; Wang, D.; Huynh, B. H.; Edmondson, D. E.; Salifoglou, A.; Lippard, S. J. *J. Am. Chem. Soc.* **1995**, *116*, 7465. (b) Liu, K. E.; Valentine, A. M.; Wang, D.; Huynh, B. H.; Edmondson, D. E.; Salifoglou, A.; Lippard, S. J. *J. Am. Chem. Soc.* **1995**, *117*, 10174. (c) Liu, K. E.; Valentine, A. M.; Qiu, D.; Edmondson, D. E.; Appelman, E. H.; Spiro, T. G.; Lippard, S. J. *J. Am. Chem. Soc.* **1995**, *117*, 4997;

(14) Wilkinson, E. C.; Dong, Y.; Zang, Y.; Fujii, H.; Fraczkiewicz, R.; Fraczkiewicz, G.; Czernuszewicz, R. S.; Qui, L. Jr. *J. Am. Chem. Soc.* **1998**, *120*, 955.

(15) Lee, S. K.; Nesheim, J. C.; Lipscomb, J. D. *J. Biol. Chem.* **1993**, *268*, 21569.

(16) Valentine A. M.; Stahl, S. S.; Lippard, S. J. *J. Am. Chem. Soc.* **1999**, *121*, 3876.
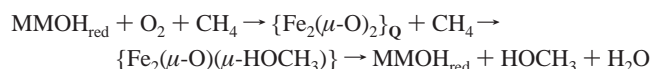
questions, here we have performed quantum chemical calculations of the structure (both geometrical and electronic) and energetics of assumed intermediates and transition states of the reaction.

Previously, several theoretical attempts[17−19] have been made to model MMOH and to study the mechanism of the MMO reaction. However, these studies used either unrealistic or small models, such as FeO^+,[17] $Fe_2(OH)_3(H_2O)_2(HCOO)(\mu\text{-}O)_2$,[18a] $Fe_2\text{-}(OH)_4(H_2O)_4(\mu\text{-}O)_2$,[18a] and $(H_2O)_2Fe(\mu\text{-}O)_2Fe(H_2O)^+$,[3,18b] or low-level theoretical models, such as the extended-Hückel method.[17] While this paper was in the final stage of preparation, a preprint by Siegbahn was received that used a more realistic model.[19] Later in the present paper, we plan to compare our results with those from previous theoretical studies.

II. Computational Procedure and Model of the Q Intermediate

Our long-term goal is to study the mechanism of the reaction

$$MMOH_{red} + O_2 + CH_4 \rightarrow \{Fe_2(\mu\text{-}O)_2\}_Q + CH_4 \rightarrow$$
$$\{Fe_2(\mu\text{-}O)(\mu\text{-}HOCH_3)\} \rightarrow MMOH_{red} + HOCH_3 + H_2O$$

In the present paper we discuss only the following part of this reaction

$$\{Fe_2(\mu\text{-}O)_2\}_Q + CH_4 \rightarrow \{Fe_2(\mu\text{-}O)(\mu\text{-}HOCH_3)\} \quad (1)$$
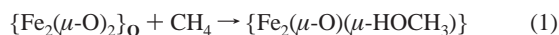
For this purpose we have to choose a reasonable model for the starting complex, **Q**. According to the experimentally available information, any working model should satisfy the following conditions: (1) It should include two Fe−Fe bridging oxo ligands, two bridging carboxylates coordinated to the two Fe centers, and one imidazole and one monodentate coordinated carboxylate ligand for each Fe center. (2) Net charge of the system should be "zero". (3) Imidazole rings of the His ligands are located cis to each other, i.e., two monodentate terminal carboxylates are cis to each other as well.

The smallest reasonable model of compound **Q** satisfying these conditions is $cis\text{-}(H_2O)(NH_2)Fe(\mu\text{-}O)_2(\eta^2\text{-}HCOO)_2Fe(NH_2)(H_2O)$, **I**, which was chosen to be our working model throughout of this paper. In our succeeding papers, to elucidate the electronic and steric/electrostatic effects from the histidine and glutamic acid residues, as well as those of protein environment, a variety of larger models satisfying the above-mentioned conditions will be adopted, employing a variety of levels of theoretical methods, including the hybrid method such as the ONIOM method.[20]

Another important question in these studies is the spin state of the system. Spectroscopic studies[4] indicate that the binuclear iron cluster of $MMOH_{ox}$ (diferric) has two $S = 5/2$ irons antiferromagnetically spin coupled to yield a diamagnetic center. The exchange coupling constant J between two Fe centers is found to be small (7 ± 3 cm^{-1}).[4] As expected, the isolated diferric MMOH ($MMOH_{ox}$) exhibits no ground-state EPR signals, but a signal from an integer spin excited state has been observed. However, differous MMOH ($MMOH_{red}$) exhibits ferromagnetic coupling of two $S = 2$ ferrous irons to give an $S = 4$ ground state, and gives an intense EPR signal at about $g = 16$. The

EXAFS studies on the $MMOH_{red}$ did not detect any significant Fe−Fe contribution, indicating that the two Fe are further apart than in the $MMOH_{ox}$, and thus may be less strongly coupled, which is consistent the reported Fe−Fe distance, 3.43 Å, slightly longer than 3.32 Å for diferric $MMOH_{ox}$. The exchange coupling constant between two Fe centers is found to be extremely small (0.35 cm^{-1}). Spectroscopic studies also show that diferryl compound **Q** is diamagnetic, suggesting that compound **Q** contains two antiferromagnetic coupled high-spin Fe^{IV} atoms. The complex is EPR silent, and the exchange coupling J constant is found to be relatively larger, >60 cm^{-1}. This is also consistent with the short, 2.46 Å, Fe−Fe distance of compound **Q**. Thus, $MMOH_{ox}$ and compound **Q** are antiferromagnetically coupled diamagnetic species, while $MMOH_{red}$ is a ferromagnetically coupled paramagnetic species. In other words, during the hydrocarbon hydroxylation reaction by MMO, one may expect spin crossing of the system, and switching between antiferromagnetic and ferromagnetic couplings among the expected intermediates and transition states.

However, for single-determinant calculations, such as density functional methods, it is difficult to represent the open-shell low-spin coupling ($2S + 1 = 0$) of the two paramagnetic centers, each having the multiplicity $2S + 1 = 5$ (Fe^{IV}, d^4) or 6 (Fe^{III}, d^5); the "restricted" calculations for the low-spin state give the closed-shell singlet state that cannot represent an open-shell atoms. An "unrestricted" calculation with low M_S value gives a heavily spin-contaminated state or the total wave function becomes symmetry broken and does not represent a true eigenstate. Therefore, to retain the proper spins on individual iron atoms, we performed spin-unrestricted open-shell single-determinant calculations for ferromagnetically coupled high-spin states with multiplicities of $2M_S + 1 = 9$ and 11, ^9A and ^{11}A, respectively. As will be discussed, the expectation values of the S^2 operator for both ^9A and ^{11}A wave functions at their various optimized geometries turned out in most cases to be not far from the pure spin eigenfunction values, and spin contamination is not a problem for these states. Since the magnitude of the spin coupling between the two centers is not strong, as discussed above, we expect that the mechanism of reaction 1 is not much influenced by the antiferromagnetical nature of the complex.

We used the hybrid density functional method, B3LYP,[21] in conjunction with the Stevens−Basch−Krauss (SBK) effective core potentials (ECP) and the standard 31G, CEP-31, and (8s8p6d/4s4p3d) basis sets for H, (C, O, and N), and Fe atoms, respectively,[22] which we call the SBK basis set, for geometry optimization. The energies were recalculated at the B3LYP/SBK optimized geometries with two polarization basis functions at the B3LYP level. SBK(O*) is the SBK basis set augmented by a polarization d function ($\alpha = 0.85$) on all the oxygen atoms except those on two terminal water molecules. The largest basis set SBK(CO*) adds to SBK(O*) a polarization d function ($\alpha = 0.75$) on the three carbon atoms of all the carboxylates and methane.

The geometries of the reactants, all intermediates, transition states (TS's), and products of reaction 1 were determined by gradient optimization using the Gaussian94 package.[23] Since the systems studied here were too large for our computer resources, second derivative calculations were not performed. To confirm the nature of the calculated TS, quasi-IRC (intrinsic reaction coordinate) calculations were carried out in the following manner. The geometry of the transition state was at first shifted, toward both the reactant and the product side, based on the eigenvector of the imaginary frequency of the approximate Hessian,

(17) (a) Yoshizawa, K.; Shiota, Y.; Yamabe, T. *Chem. Eur. J.* **1997**, *3*, 1160. (b) Yoshizawa, K.; Shiota, Y.; Yamabe, T. *J. Am. Chem. Soc.* **1998**, *120*, 564. (c) Yoshizawa, K.; Shiota, Y.; Yamabe, T. *Organometallics* **1998**, *17*, 2825.

(18) (a) Siegbahn, P. E. M.; Crabtree, R. H. *J. Am. Chem. Soc.* **1997**, *119*, 3103. (b) Yoshizawa, K.; Ohta, T.; Yamabe, T. *Bull Chem. Soc. Jpn.* **1998**, 71, 80862. (c) Siegbahn, P. E. M.; Crabtree, R. H.; Nordlund P. J. *Biol. Inorg. Chem.* **1998**, *3*, 314.

(19) Siegbahn, P. E. M. *Inorg. Chem.* **1999**, *38*, 2880.

(20) (a) Maseras, F.; Morokuma, K. *J. Comput. Chem.* **1995**, *16*, 1170. (b) Humbel, S.; Sieber, S.; Morokuma, K. *J. Chem. Phys.* **1996**, *105*, 1959. (c) Svensson, M.; Humbel, S.; Froese, R. D. J.; Matsubara, T.; Sieber, S.; Morokuma, K. *J. Phys. Chem.* **1996**, *100*, 19357. (d) Dapprich, S.; Komaromi, I.; Byun, K. S.; Morokuma, K.; Frisch, M. J. *J. Mol. Struct. (THEOCHEM)* **1999**, *461−462*, 1.

(21) (a) Becke, A. D. *Phys. Rev. A* **1988**, *38*, 3098. (b) Becke, A. D. *J. Am. Chem. Soc.* **1993**, *98*, 1372. (c) Becke, A. D. *J. Chem. Phys.* **1993**, *98*, 5648. (d) Lee, C.; Yang, W.; Parr, R. G. *Phys. Rev. B* **1988**, *37*, 785.

(22) (a) Stevens, W. J.; Basch, H.; Krauss, M. *J. Chem. Phys.* **1984**, *81*, 6026. (b) Stevens, W. J.; Krauss, M.; Basch, H.; Jasien, P. G. *Can. J. Chem.* **1992**, *70*, 612.

(23) Gaussian 94, Revision D.3, Frisch, M. J.; Trucks, G. W.; Schlegel, H. B.; Gill, P. M. W.; Johnson, B. G.; Robb, M. A.; Cheeseman, J. R.; Keith, T. A.; Petersson, J. A.; Montgomery, J. A.; Raghavachari, K.; Al-Laham, M. A.; Zakrzewski, V. G.; Ortiz, J. V.; Foresman, J. B.; Cioslowski, J.; Stefanov, B. B.; Nanayakkara, A.; Challacombe, M.; Peng, C. Y.; Ayala, P. Y.; Chen, W.; Wong, M. W.; Andres, J. L.; Replogle, E. S.; Gomperts, R.; Martin, R. L.; Fox, D. J.; Binkley, J. S.; DeFrees, D. J.; Baker, J.; Stewart, J. J. P.; Head-Gordon, M.; Gonzales, C.; Pople, J. A.; Gaussian Inc.: Pittsburgh, PA, 1995.

Table 1. Total (in italics, in hartrees) and Relative (in kcal/mol, relative to the reactants) Energies of Various Intermediates and Transition States, for Spin Multiplicities of $2M_S + 1 = 9$ and 11, for the Reaction of MMO with Methane, Calculated at the B3LYP Level of Theory Using Different Basis Sets, SBK, SBK(O*), and SBK(CO*)

		total and relative energies			$\langle S^2 \rangle$
structures		SBK	SBK(O*)	SBK(CO*)	SBK
		⁹A state			
reactants	**I_9** + CH₄	*−419.643935*	*−419.720129*	*−419.775082*	20.15
CH₄ complex	**II_9**	−0.8	−0.7	−0.7	20.15
TS1 (C−H)	**III_9**	14.3/19.7[a]	19.6	19.5	20.91
CH₃ complex	**IV_9**	6.8	11.4	11.4	21.11
TS2 (O−CH₃)	**V_9**	17.5	18.5	18.2	20.89
CH₃OH complex	**VI_9**	−26.8	−27.9	−31.4	20.05
		¹¹A state			
reactants	**I_11** + CH₄	*−419.635119*	*−419.705552*	*−419.761075*	
		0.0	0.0	0.0 (8.8)[b]	30.16
CH₄ complex	**II_11**	−0.6	−0.3	−0.3 (8.5)	30.19
TS1 (C−H)	**III_11**	13.6/18.3[a]	14.2/18.0	14.4 (23.2)/18.3	30.15
CH₃ complex	**IV_11**	1.6	2.6	3.0 (11.8)	30.13
TS2 (O−CH₃),	**V_11**	10.9	8.8	8.8 (17.6)	30.15
CH₃OH complex	**VI_11**	−44.3	−44.8	−48.6 (−39.8)	30.03

[a] The numbers after the slash correspond to the C−H bond activation on the O¹ atom, located on the same side with water ligands. [b] In parentheses, relative to **I_9**.

and released for equilibrium optimization. In this manner, each transition state was "connected" to the reactant and the product of the respective step.

The energies given here and discussed below do not include zero-point energy correction (ZPC) or any other spectroscopic or thermodynamic terms. Note that below we will discuss only the energetics calculated at our best B3LYP/SBK(CO*) level using B3LYP/SBK optimized geometries. As one can see from Table 1, SBK and SBK-(O*) basis sets provide qualitatively the same results as those with SBK-(CO*). However, the calculated relative energies can differ up to 5 kcal/mol. The main differences appear upon going from SBK to the SBK(O*) or SBK(CO*) basis sets, especially for the ⁹A state. The general tendency is that an improved basis set increases the methane C−H bond activation barrier relative to the methane complex, makes the C−H activation reaction more endothermic, and increases the exothermicity of the methanol formation reaction.

III. Results and Discussion

The geometries of the reactants, intermediates, and transition states calculated at the B3LYP/SBK level are shown in Figure 1. Their energies calculated at the B3LYP level with different basis sets, SBK, SBK(O*), and SBK(CO*), are presented in Table 1.

Reactant Complex, I. Let us start our discussions with the reactant, compound **I**, which is a model of compound **Q** reported experimentally.[4b] As seen from Figure 1, the calculated geometric parameters and the general structural character of compound **I**, which can be formally written as L₄Fe(μ-O)₂FeL₄, are consistent with the experimental findings.[3,4,11,12] Namely, the full geometry optimization of the proposed model without any symmetry constraint shows that it has two "μ-oxo" (or so-called "diamond" core oxygen) atoms and two bidentate carboxylate ligands coordinated to the Fe centers. Furthermore, the "diamond core" Fe₂O₂ of structures **I**, as in the experimentally reported compound **Q**, has an asymmetric structure; one of the diamond core O atoms is located closer to one Fe center, and the second one is closer to the other Fe center. The calculated short bond distances, Fe¹−O² and Fe²−O¹, are 1.729 and 1.785 Å for the **I_9** state and 2.013 and 1.737 Å for the **I_11** state, respectively, and are in fair agreement with the experimentally reported[4b] value of 1.77 Å in compound **Q**. Similarly, the calculated long bond distances, Fe¹−O¹ and Fe²−O², 1.921 and 2.019 Å for the **I_9** state and 2.185 and 2.107 Å

for the **I_11** state, respectively, are in reasonable agreement with the experimental[4b] value of 2.05 Å in compound **Q**. Clearly, the calculated diamond Fe−O distances in **I_9** are a better match to the experimental values than **I_11**. This agrees with the experimental assignment of the **Q** structure as having two ferryl Fe^IV atoms each with d⁴ electronic configurations and a total of 8 unpaired spins. However, the Fe−Fe distances, 2.692 and 2.945 Å, calculated for the **I_9** and **I_11** states, respectively, are 0.23 and 0.50 Å longer than the experimentally[4b] reported value, 2.46 Å. This large discrepancy between the calculated and the experimental value of the Fe−Fe distance most likely is a result of the use of a ferromagnetic coupling scheme in our calculations. Recent results reported by Siegbahn[19] for an antiferromagnetic coupled singlet state give a shorter Fe−Fe distance, although the validity of the density functional calculation to describe the antiferromagnetic coupling state can be strongly questioned, as discussed in Section II.

Methane−Q Complex, II. The next step of the reaction is expected to be coordination of the incoming substrate to compound **I**. As seen in Figure 1, in general, two distinct pathways, **O**-site and **N**-site, corresponding to the substrate coordination to the bridging oxygen atoms, O¹ and O², located on the H₂O and NH₂ sites, respectively, are possible. According to experimental data,[4] the only valid pathway is a coordination of substrate from the O side, because of the existence of the substrate coordination pocket; the coordination of substrate from the N side is sterically hindered and is not available. Despite that, in this paper we investigated only the N-side pathway, since a preliminary calculation suggested that this side may be more reactive. We are presently studying reaction pathway on the O side, which will be reported separately. Here, let us only say that the O-side pathway looks qualitatively similar to the N-side pathway.

The first step of the reaction is expected to be coordination of the incoming substrate to compound **I**. Our extensive search shows that coordination of the methane molecule to one of the diamond O atoms is more favorable than any other potentially possible coordination modes. As seen in Figure 1, coordination of the methane molecule to compound **I** leads to the methane−**Q** complex, structure **II**. Since the interaction between methane and structure **I** is extremely weak, the geometries of the CH₄ and **I** fragments in complex **II** are very close to those in the free CH₄ and **I**, respectively. The complexation energy is

Methane → Methanol Conversion Reaction Mechanism

J. Am. Chem. Soc., Vol. 121, No. 31, 1999 7253
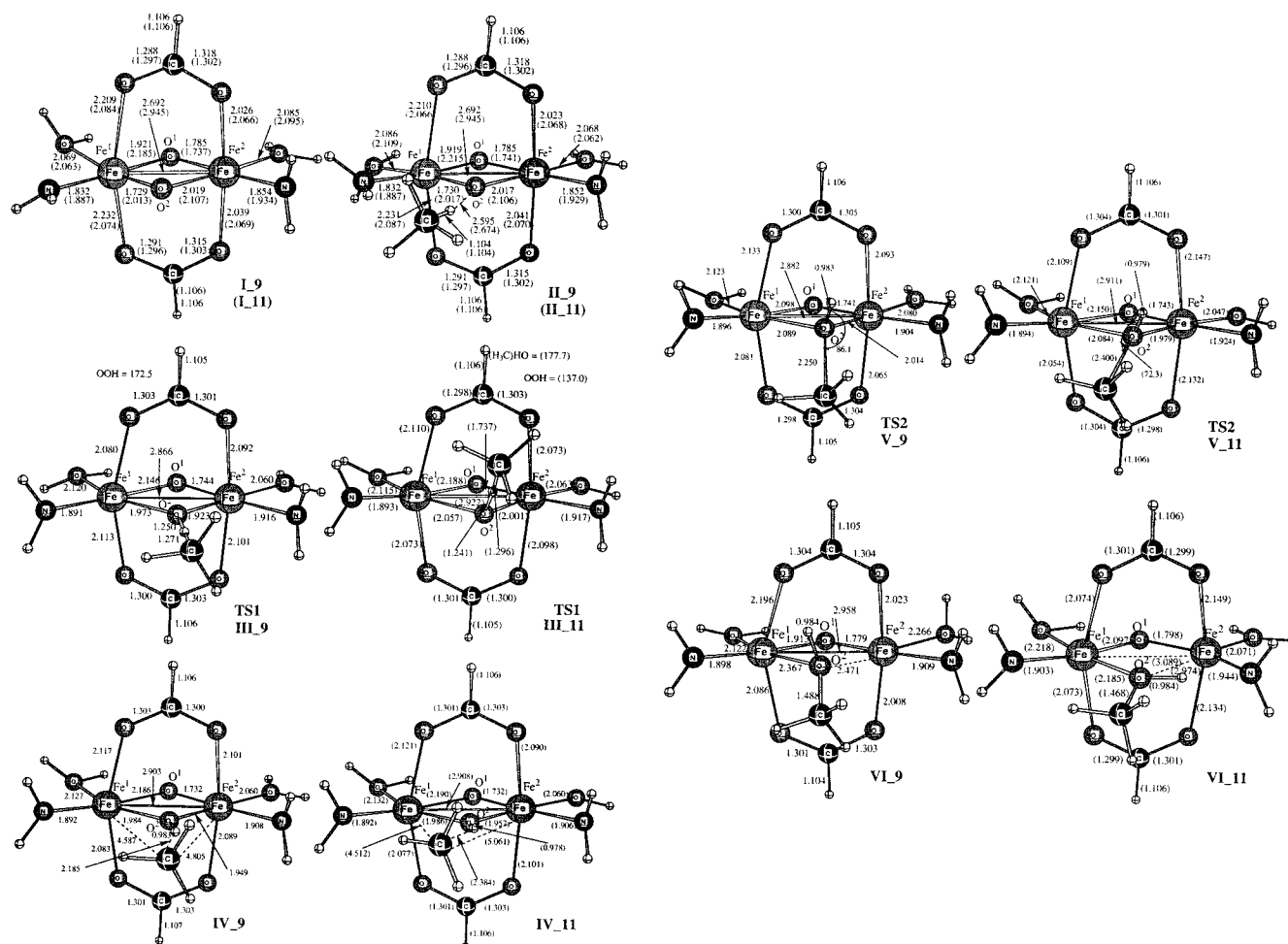
Figure 1. The calculated structures (distances in Å, angles in deg) of the intermediates and transition states of the following reaction: (NH_2)-$(H_2O)Fe(\mu\text{-}O)_2(\eta^2\text{-}HCOO)_2Fe(NH_2)(H_2O) + CH_4 \rightarrow (NH_2)(H_2O)Fe(\mu\text{-}O)(\mu\text{-}HOCH_3)(\eta^2\text{-}HCOO)_2Fe(NH_2)(H_2O)$. Numbers for the ^9A state are without parentheses and those for the ^{11}A state are in parentheses.

Table 2. Mulliken Atomic Spin Densities (in e) for the Various Intermediates and Transition States of the MMO + Methane Reaction, Calculated at the B3LYP/SBK Level

structures	atomic spin densities (in e)					
	Fe^1	Fe^2	O^1	O^2	H^a	CH_3^b
I_9	3.17	3.37	0.33	0.45		
II_9	3.16	3.36	0.31	0.45		
III_9	3.40	4.09	0.56	−0.22	0.03	−0.46
IV_9	3.32	4.15	0.59	0.19	0.00	−0.98
V_9	3.28	4.14	0.50	0.21	0.00	−0.81
VI_9	2.80	4.15	0.35	0.04	0.00	0.00
I_11	3.35	4.10	0.57	1.21		
II_11	3.37	4.10	0.58	1.21		
III_11	3.35	4.12	0.59	0.74	−0.05	0.52
IV_11	3.34	4.14	0.59	0.22	0.02	1.00
V_11	3.61	4.14	0.55	0.10	0.00	0.85
VI_11	4.10	4.13	0.57	0.05	0.00	0.00

^{a} H atom located between O^2 and CH_3 fragments. ^{b} The number for the entire CH_3 fragment.

calculated (relative to the corresponding reactants) to be 0.7 and 0.3 kcal/mol for the ^9A and ^{11}A states, respectively. Because of unfavorable zero-point energy and entropy factors, it is most likely that this CH_4 compound **Q** complex **II** does not exist in reality, and therefore we will not discuss it in detail.

In Table 2 we have presented the calculated Mulliken spin densities (populations, to be more exact) of selected atoms for the optimized structures. In structures **I**, as seen in the table, of the total of eight unpaired electrons (spins) of the ^9A state roughly six and a half are localized on two Fe atoms, a half of the remaining 1.5 unpaired electrons is located on the bridging O atoms, and the rest is distributed on the noncore ligands. In the ^{11}A state with 10 unpaired electrons, the spin densities on the Fe centers are increased by one and those on the bridging O centers are also increased by one, while the spin densities on the noncore ligands change little, indicating that the $^9A \rightarrow {}^{11}A$ transition corresponds to moving one electron from a weakly Fe−O bonding orbital of the Fe_2O_2 core to its weakly antibonding (or nonbonding) partner. Upon going from ^9A to ^{11}A, the electron density is moved mainly from Fe^2 (and O^2) to Fe^1 and O^1 (and other ligands) and the $Fe^1−O^2$ and $Fe^1−O^1$ bonds are elongated much more than other Fe−O bonds of the Fe_2O_2 diamond core. Even though the "formal oxidation state" is not very practical when a large fraction of spins is delocalized, one may consider **I_9** (and **II_9**) in the ^9A state very qualitatively to have $Fe^{IV}−Fe^{IV}$ with four spins each which are partly delocalized to the bridge oxygen and other ligands. On the other hand, **I_11** (and **II_11**) in the ^{11}A state is in the $Fe^{IV}−Fe^{III}$ mixed valence state, where Fe^2 is in the Fe^{III} state with five spins which are heavily delocalized onto O^2. The calculated fact that **I_9** is lower in energy than **I_11** suggests that $Fe^{IV}−Fe^{IV}$ is the preferred state for complex **I**. This is consistent with the experimental indications that complex **Q** is likely to be in the $Fe^{IV}−Fe^{IV}$ state.

Transition State, III, and Product, IV, for C—H Activation. The activation of the methane C—H bond is found most likely to take place on the diamond oxygen O^2 located on the same side with the imine ligands. Our extensive attempts to find other possible pathways for methane C—H activation either converged to the transition states **III_9** and **III_11** for the ^9A and ^{11}A states, respectively, or led to the transition states higher in energy than structures **III_9** and **III_11**, respectively. For instance, the coordination of the CH_4 molecule to (i) the diamond O^2 and Fe^1 centers simultaneously with its C—H bond and (ii) only the Fe^1 without and with lifting one of the Fe^1—O (carboxylate) bonds all lead to TS **III_9** and **III_11**.

As seen from Figure 1, in transition states **III_9** and **III_11** the C—H bond to be broken is elongated from 1.104 Å in **II** to 1.271 and 1.296 Å for the ^9A and ^{11}A states, respectively. Furthermore, the O—H bond is nearly formed, with 1.250 and 1.241 Å at the TS's, compared to 0.983 and 0.978 Å in the products **IV_9** and **IV_11**, respectively. The "quasi-IRC" calculations, as mentioned in Section II, confirmed that structure **III_9** (or **III_11)** is the true transition state connecting **II_9** (or **II_11**) with **IV_9** (or **IV_11**). Comparison of the **III_9** and **III_11** structures shows that the geometries of their active parts are very similar, with an exception of that in the **III_9** CH_4 unit located on the FeOOFe plane, while in the **III_11** it is bent up by 49°.

The geometrical parameters indicate clearly that **III_9** and **III_11** are the TS's corresponding to the H abstraction process for the ^9A and ^{11}A states, respectively. The H-abstraction barriers are calculated to be 19.5 and 14.4 kcal/mol for the ^9A and ^{11}A states, respectively, relative to the corresponding CH_4 complexes **II_9** and **II_11**, respectively. These values of the barrier are in reasonable agreement with available experimental estimates, 14—18 kcal/mol.[16] The present results of the reaction pathway agree qualitatively with those of Siegbahn,[19] although his barrier is substantially lower (7.1 kcal/mol, including ZPC) than our values.

The spin densities in Table 2 for compounds **III** and **IV** are found to be similar to each other within their respective ^9A and ^{11}A states. Furthermore, the spin densities are nearly identical between ^9A and ^{11}A, except for those on the O^2··H··CH_3 fragment. For the CH_3 group itself, the total Mulliken charge (not shown in Table 2) is at most +0.03 for both the ^9A and ^{11}A states and the spin densities on this group for ^9A and ^{11}A are of the same magnitude but of opposite sign. One can interpret all these values in the following way. In both TS's, **III_9** and **III_11**, a radical center begins to develop on the CH_3 group, with spin densities of −0.46 and +0.52, respectively, and in both intermediates, **IV_9** and **IV_11**, the CH_3 group is now a real radical with spin densities of −0.98 and 1.00, respectively. The spin densities on Fe^1 and Fe^2 in **IV_9** and **IV_11** can qualitatively be considered to correspond to Fe^{IV} with four spins and Fe^{III} with five spins, respectively. In going from **II_9** to **III_9**, the very qualitatively formal oxidation state of Fe^2 changes from Fe^{IV} to Fe^{III}, while from **II_11** (which is already Fe^{III}) to **III_11**, no such change is required. Since the two Fe centers are coupled ferromagnetically in both ^9A and ^{11}A states, the spin of the CH_3 radical in both **III** and **IV** has to couple antiferromagnetically (with negative spin) and ferromagnetically (with position spin) to make the total spin $2M_S + 1$ equal to 9 and 11, respectively. In the bound radical complexes **IV_9** and **IV_11**, in which the interaction of the CH_3 radical with the two iron atoms is very weak, the total energies are nearly identical and the optimized geometries in Figure 2 are
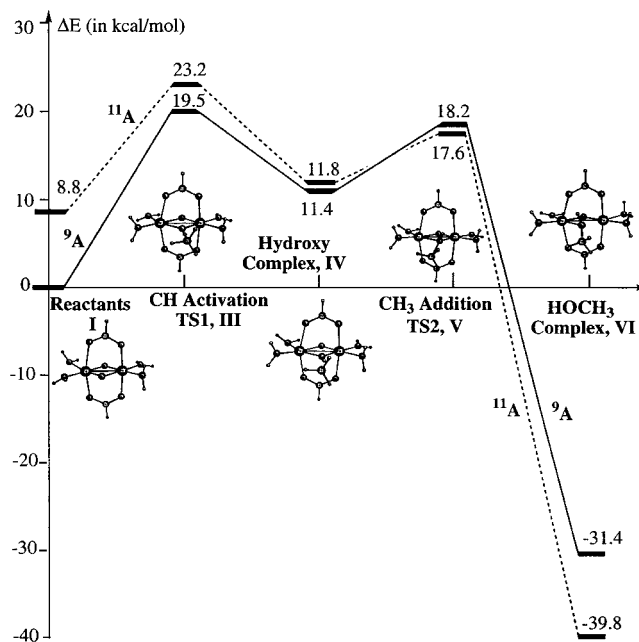
Figure 2. The potential energy profile (in kcal/mol) at the B3LYP/SBK(CO*)//B3LYP/SBK level for both the ^9A state and the ^{11}A state of the methane activation reaction: $(NH_2)(H_2O)Fe(\mu\text{-}O)_2(\eta^2\text{-}HCOO)_2\text{-}Fe(NH_2)(H_2O) + CH_4 \rightarrow (NH_2)(H_2O)Fe(\mu\text{-}O)(\mu\text{-}HOCH_3)(\eta^2\text{-}HCOO)_2\text{-}Fe(NH_2)(H_2O)$.

also nearly identical. In the transition states **III_9** and **III_11** where the spin is about 50% developed, the energies and geometries are similar. The fact that the system wants to adopt the same structures, regardless of whether the overall spin state $2M_S + 1 = 9$ or 11, suggests that this mixed spin Fe^{IV}—Fe^{III} electronic configuration is the preferred state of intermediate **IV**. It is quite interesting that we find that a mixed valence state is responsible for the methane oxidation reaction. The present spin density analysis clearly demonstrates that the methane oxidation proceeds via a bound-radical mechanism, which is in good qualitative agreement with the radical clock probe experiments of Lippart et al.[24] on the oxidizing of ethane and butane, where it was shown only 71—78% of reaction takes place with retention of configuration.

In these product structures **IV_9** and **IV_11**, as seen in Figure 1, the Fe centers are bridged by one O and one OH ligands. **IV** is a oxo—hydroxyl complex, formally written as $L_4Fe(\mu\text{-}O)(\mu\text{-}OH)FeL_4$, with the methyl radical only weakly interacting via a C··HO interaction. The Fe^1—O^1 bond elongates from 1.919 to 2.186 Å, while the Fe^2—O^1 bond is shortened from 1.785 to 1.732 Å, upon going from **II_9** to **IV_9**. The corresponding changes are less significant for structures **II_11** and **IV_11**. The Fe^1—O^2H and Fe^2—O^2H bonds are 1.984 and 1.949 Å in structure **IV_9**, compared to the corresponding Fe—O distance of 1.730 and 2.017 Å in structure **II_9**; the asymmetry of the Fe—OH distance in **IV_9** is much smaller than that in the Fe—O distance in **II_9**. A similar reduction of asymmetry is also seen between **II_11** and **IV_11**.

The entire process $I + CH_4 \rightarrow IV$ is calculated to be endothermic by 11.4 and 3.0 kcal/mol, for the ^9A and ^{11}A states, respectively. These numbers are in fair agreement with Siegbahn's latest 2.3 kcal/mol[19] and previous 1.2 kcal/mol,[18a] both for the $2M_S + 1 = 9$ state. The general conclusion from the above-presented results is that the MMO-catalyzed methane

(24) Valentine, A. M.; Wikinson, B.; Liu, K. E.; Komar-Panicucci, S.; Priestley, N. D.; Williams, P. G.; Morimoto, H.; Floss, H. G.; Lippard, S. J. *J. Am. Chem. Soc.* **1997**, *119*, 1818.

hydroxyl-ation reaction occurs via a "bound-radical" mechanism. Siegbahn et al.[18a] in their earlier paper using a smaller model with 5-coordinate Fe atoms also concluded that reaction takes place via a radical mechanism. However, they concluded that H-atom abstraction from methane takes place on the terminal oxo ligand, and the reaction rapidly leads to formation of a weak Fe$-$CH$_3$ bond. However, our calculations could not confirm these conclusions; first, we were unable to find the Fe$-$methyl complex, and second, the hydrogen abstraction takes place on the bridged O-center rather than terminal oxo-center. The discrepancy between our and their results can be due to the relatively small model used in their calculations. Indeed, their latest results[19] using a more realistic model are consistent with our results, although they still could not entirely rule out the formation of the Fe$-$CH$_3$ bond.

Our results, as well as Siegbahn's latest work, differ both qualitatively and quantitatively from those by Yoshizawa and co-workers.[17] They used the naked FeO$^+$ as a model for MMO and found a four-center transition state involving O, Fe, C, and H atoms, leading to the hydroxy$-$methyl$-$Fe, (OH)FeCH$_3$$^+$, complex, where the entire process is 41 kcal/mol exothermic. Therefore, their mechanism can be classified as a nonradical mechanism. Furthermore, the complexation energy of methane to compound **Q** (in this paper compound **I**) is very small in our as well as Siegbahn's[19] latest calculations, while it is extremely large (19.5 kcal/mol) for naked FeO$^+$. The present disagreement clearly indicates that naked FeO$^+$ is a very poor model for MMO for the methane hydroxylation process.

Transition State, V, and Product, VI, for Methanol Formation. The next step in the reaction path should be the reaction of the methyl radical with the complex, which is found to occur via transition states **V_9** and **V_11**, for the ^{9}A and ^{11}A states, respectively. Figure 1 reveals that this transition state involves a torsion motion of the hydroxyl OH ligand before the methyl radical can add to the bridging hydroxyl ligand to form methanol. As the methyl radical approaches from below the core Fe^{1}O^{1}Fe^{2}O^2 plane to the hydroxyl ligand O^{2}H, the H atom of the latter leaves the coplanar tricoordinate O environment and bends upward, to create a tetrahedral tetracoordinate O environment. Apparently this bend costs some energy, before gaining it back by reaction of the methyl group to form a C$-$O covalent bond. The barrier heights for the CH$_3$ addition to the hydroxyl ligand calculated relative to the intermediate **IV_9** and **IV_11** are 6.8 and 5.8 kcal/mol for the ^{9}A and ^{11}A states, respectively. Obviously, this step of the reaction is not rate-determining, and can occur rather fast; the lifetime of the radical intermediate is expected to be too short to be detected experimentally.

Overcoming the barriers at **V_9** and **V_11** leads to the complexes **VI_9** and **VI_11**, which can be written as a methanol complex L$_4$Fe(OHCH$_3$)(μ-O)FeL$_4$ with H and methyl groups bound to the same oxygen atom (O^2) of the Fe$_2$O$_2$ diamond core. As seen in Figure 1, upon reaction of the methyl group with the diamond HO^2 group, the Fe^2$-$O^2 bond is elongated to 2.471 and 2.974 Å at structures **V_9** and **V_11**, respectively, indicating that they are already broken. At the same time, the Fe^1$-$O^2 bond is weakened significantly too, from 1.984 Å in **IV_9** to 2.367 Å in **VI_9**, and from 1.986 Å in **IV_11** to 2.185 Å in **VI_11**. The elongation of the Fe^2$-$O^{2}H(CH$_3$) bond prepares the system to the next step, elimination of the methanol molecule and regeneration of the enzyme. The overall reaction **I** + CH$_4$ → **VI** is calculated to be exothermic by 31.4 and 48.6 kcal/mol for the ^{9}A and ^{11}A states, respectively.

Table 2 shows that in the ^{11}A state upon going from the hydroxyl complex **IV_11** to the methanol complex **VI_11**, Fe^1 changes its formal oxidation state from Fe^{IV} with four spins to Fe^{III} with five spins, while the spin density on the methyl radical is completely annihilated upon forming a covalent bond between CH$_3$ and OH. The transition state **V_11** has a spin distribution between that of **IV_11** and **VI_11**. On the other hand, in the ^{9}A state upon going from the hydroxyl complex **IV_9** to the methanol complex **VI_9**, the spin density on Fe^1 is reduced by about 0.5, corresponding to the disappearance of roughly one unpaired electron. Since Fe^V is not a stable species, it is most likely Fe^1 changed its formal oxidation state from Fe^{IV} with four spins to Fe^{III} with five formal d electrons. Because of the restriction $2M_S + 1 = 9$, i.e., the total number of unpaired electrons must be 8 within the Fe^{III}$-$Fe^{III} core, Fe^1 in **VI_9** chose to form one d lone pair with only three spins remaining. This complex **VI_9** is thus higher in energy than the corresponding complex **VI_11** in violation of the Hund rule.

The final step of elimination of the methanol molecule and regeneration of the enzyme could be a complex process, and there exists the possibilities of different mechanisms. It could occur via a stepwise mechanism, which starts with elimination of the methanol molecule leading CH$_3$OH and an intermediate with the Fe$-$O$-$Fe core, and then later the latter can eliminate the water molecule and regenerate enzyme through a 2-electron reduction. Another stepwise mechanism can start with the 2-electron reduction process of the bridging O^1 atom to give a water molecule, followed by elimination of methanol and regeneration of the enzyme. Also possible is the concerted mechanism, where elimination of the methanol occurs spontaneously with 2-electron reduction of the bridging O^1-center and regeneration of the enzyme. A mechanism starting from one-electron reduction followed by methanol elimination cannot be excluded. Studies on these mechanisms are in progress and will be reported separately.

The Full Potential Energy Profile and Interplay between Multiplicity $2M_S + 1 = 9$ and 11 Pathways. Finally, let us discuss the entire potential energy profiles for both ^{9}A and ^{11}A states, as shown in Figure 2, compare the energetics, and discuss the interplay between the ^{9}A and ^{11}A states for the reactants, intermediates, transition states, and products of the reaction **I** + CH$_4$ → **VI**. An important finding is that the potential energy profile does not differ much between the ^{9}A and ^{11}A states. In both states, the reaction proceeds from **I** (model of **Q**) via C$-$H activation on one of the bridging O atoms, which is the rate-determining step, and is followed by the formation of methanol between the methyl radical and the bridged OH group.
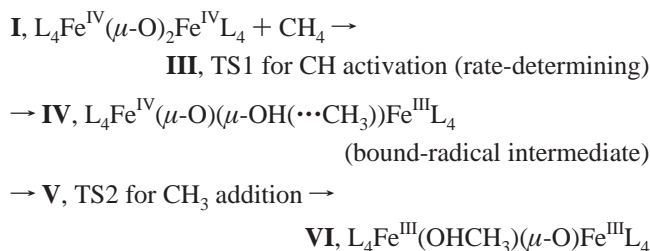
When examined in detail, there are some differences in the energetics between the two states and one can see clear changes in the preferred electronic states of the Fe core as the reaction proceeds. At reactant **I**, the ^{9}A state is lower than the ^{11}A state by 8.8 kcal/mol, which is reduced to 3.7 kcal/mol at the TS1 **III**. The ^{9}A state of **I** has, qualitatively speaking, an Fe^{IV}$-$Fe^{IV} core, as suggested experimentally for **Q**, while the ^{11}A state of **I** has an Fe^{IV}$-$Fe^{III} core and is less stable. Since the coupling between two Fe cores is rather weak, the use of ferromagnetic coupling between two irons in the calculation is not likely to distort the energetics of different formal oxidation states of the two irons. Therefore, our calculated results with the ferromagnetic Fe$-$Fe coupling are expected to be similar to the results which would be obtained for the antiferromagnetic coupling (as is found experimentally for complex **Q**), since the formal electronic structure of each Fe center is described properly. Once

the system reaches the hydroxyl complex **IV**, calculations for both ^{9}A and ^{11}A converge to the same electronic state with the same structure and energy, corresponding to the Fe^{IV}−Fe^{III} mixed valence state that is interacting weakly with the methyl radical either ferro- or antiferromagnetically. In the product methanol complex **VI**, the ^{11}A state is 8.4 kcal/mol lower than the ^{9}A state. Here, the preferred iron core is Fe^{III}−Fe^{III} and each Fe has five spins, which naturally gives the ^{11}A state when ferromagnetically coupled.

IV. Conclusions

From the above presented results and discussions, one may draw the following conclusions.

1. The MMO-catalyzed methane hydroxylation reaction proceeds via a bound-radical mechanism. The reaction starts from the bis(μ-oxo) compound **I** (model of **Q**) and goes over the rate-determining transition state **III** for H abstraction from methane to the form a (μ-O)(μ-OH) intermediate **IV,** which is complexed weakly with a methyl radical. This intermediate **IV** is presumably short-lived and is not likely to be easily detected experimentally, as it is converted via a low barrier at transition state **V** for the addition of this methyl radical to the μ-OH ligand to produce the oxo−methanol complex **VI**. During the process, the oxidation state of the Fe core changes from Fe^{IV}−Fe^{IV} in **I** to a mixed valence Fe^{IV}−Fe^{III} in short-lived intermediate **IV**, and finally to Fe^{III}−Fe^{III} in **VI**. These intricate changes of formal oxidation state must provide some of the driving force for the catalysis.

I, $L_4Fe^{IV}(\mu\text{-O})_2Fe^{IV}L_4 + CH_4 \rightarrow$

$\qquad$ **III**, TS1 for CH activation (rate-determining)

$\rightarrow$ **IV**, $L_4Fe^{IV}(\mu\text{-O})(\mu\text{-OH}(\cdots CH_3))Fe^{III}L_4$

$\qquad\qquad\qquad$ (bound-radical intermediate)

$\rightarrow$ **V**, TS2 for CH$_3$ addition $\rightarrow$

$\qquad\qquad$ **VI**, $L_4Fe^{III}(OHCH_3)(\mu\text{-O})Fe^{III}L_4$

2. By comparing our results with Siegbahn's old model and Yoshizawa's FeO$^+$ model studies, it can be concluded that (a) the desired model of MMO should include bridging carboxylate ligands and (b) naked FeO$^+$ is a very poor model of MMO.

Supporting Information Available: Tables of optimized geometries (PDF). This material is available free of charge via the Internet at http://pubs.acs.org.

JA9906296